Nuclear Instruments and Methods in Physics Research A 762 (2014) 119–124

Contents lists available at ScienceDirect

Nuclear Instruments and Methods in Physics Research A

journal homepage: www.elsevier.com/locate/nima

Characterization of a mid-sized Li foil multi-wire proportional counter neutron detector

Kyle A. Nelson [a,*], Michael R. Kusner [b], Benjamin W. Montag [a], Michael R. Mayhugh [b], Aaron J. Schmidt [a], Clayton D. Wayant [a], J. Kenneth Shultis [a], Philip B. Ugorowski [a], Douglas S. McGregor [a]

[a] S.M.A.R.T. Laboratory, Mechanical and Nuclear Engineering, Kansas State University, Manhattan, KS 66506, USA
[b] Saint-Gobain Crystals, Hiram, OH 44234, USA

ARTICLE INFO

Article history:
Received 29 October 2013
Received in revised form
3 April 2014
Accepted 5 May 2014
Available online 27 May 2014

Keywords:
Helium-3 replacement
Neutron detector
Multi-wire proportional counter
Li foil

ABSTRACT

A 550 cm^2 thermal neutron detector was constructed with five parallel sheets of 75 μm thick ^{6}Li foil (95% enrichment) spaced 1.63 cm apart. Anode wire banks containing a plurality of anode wires were strung on both sides of each foil, six banks in total. The chamber was backfilled with P-10 proportional gas and over-pressured to 1.1, 1.5, 2.0, and 2.8 atm (111, 151, 202, and 284 kPa). The design was tailored to allow the products from the ^{6}Li(n,t)^{4}He reaction to escape both sides of the Li foil simultaneously, thereby, allowing for concurrent measurement in the proportional gas. The measured intrinsic thermal neutron detection efficiency of the detector with normal incident thermal neutrons to the foil sheets was $53.8 \pm 0.20\%$. When the detector was angled (55° from normal) such that a 0.5 cm diameter thermal neutron beam intersected all of the foil layers, the intrinsic thermal neutron detection efficiency increased to $58.6 \pm 0.21\%$. A ^{252}Cf neutron source positioned at a distance of 2.0 m yielded an absolute neutron detection efficiency of 0.73 cps ng^{-1}. The gamma-ray rejection ratio (GRR) was 7.67×10^{-9} as measured from a ^{60}Co source for an exposure rate of 40 mR hr^{-1}. Theoretical pulse-height spectra obtained with MCNP6 agreed well with experimental data and allowed pulse-height spectra and discriminator settings to be energy-calibrated. These results demonstrate the potential for the Li foil multi-wire proportional counter (MWPC) as a viable ^{3}He neutron detector replacement.

1. Introduction

The relatively recent shortage of ^{3}He gas has raised interest in alternative neutron detection technologies. Recently, a new category of gas-filled detectors has been introduced that utilizes solid ^{6}Li neutron absorbers configured to allow all ^{6}Li(n,t)^{4}He reaction products to escape the absorber concurrently into a proportional gas [1,2]. The Kansas State University (KSU) Semiconductor Materials And Radiological Technologies Laboratory (S.M.A.R.T. Lab) has developed a large-area, high-efficiency, low-cost, ^{6}Li foil multi-wire proportional counter (MWPC) that successfully demonstrates an acceptable alternative to ^{3}He-based neutron detector technology. A Li foil MWPC with dimensions and effective areas described here can also be used as backpack neutron detectors. Increasing the effective area of the device will allow the technology to be used in radiation portal monitors (RPMs)

Commercially available neutron detectors based on coated surfaces are restricted to the measurement of only one reaction product per neutron absorption because the other reaction product, moving in the opposite direction, deposits its energy in the device wall. An obvious example of this is the ^{10}B-lined counter, whose pulse-height spectrum is dominated by the 'wall-effect'. The consequences of the wall-effect result in lower neutron detection efficiency and poor gamma-ray discrimination [3,4]. Adequate gamma-ray discrimination can be achieved with these devices, but a large percentage of the neutron counts must be sacrificed in order to achieve acceptable gamma-ray rejection ratios (GRR). Neutron detectors filled with a neutron absorbing gas can measure both reaction products simultaneously which enhances the detection efficiency and gamma-ray discrimination properties, but ^{3}He gas is in short supply and $^{10}BF_3$ gas is considered hazardous. Single-crystal scintillator materials can have high neutron detection efficiency, but suffer from both limited size and limited gamma-ray discrimination capability [3,4]. Gamma-ray rejection can be improved for some of these materials with the use of pulse shape discrimination (PSD) [5]. This PSD approach extends also to powdered scintillator sheets

* Corresponding author.
E-mail address: knelson1@ksu.edu (K.A. Nelson).

http://dx.doi.org/10.1016/j.nima.2014.05.078
0168-9002/

that are read out by adjacent wavelength-shifting fibers. However, the necessary electronics for PSD is an additional cost.

The general design approach of the MWPC neutron detector is to suspend thin Li foils between anode wire banks, thus allowing for measurement of reaction products on both sides of the Li foil. This method takes advantage of the immediate availability of thin lithium foils, a fortuitous consequence of advancements in Li-ion battery manufacturing. Other neutron reactive materials can be used in place of ^{6}Li, but all result in lower neutron detection efficiency and reduced effective areas. The microscopic thermal-neutron (0.0259 eV) absorption cross-sections for ^{6}Li is 940 b and has a natural abundance of 7.59%. Enriched ^{6}Li has a density of 0.463 g cm^{-3} and a macroscopic thermal neutron absorption cross-section of 43.56 cm^{-1} [3,4,8]. The ^{6}Li(n,t)^{4}He reaction leads to the following products, with a reaction Q-value of 4.78 MeV [3,4,8],

$$^6\mathrm{Li}+{}^1_0n \rightarrow {}^3\mathrm{H}(2.73\ \mathrm{MeV})+\alpha(2.05\ \mathrm{MeV}). \quad (1)$$

Herein, layout and performance are reported of a 550 cm^2 ^{6}Li foil MWPC neutron detector containing 5 layers of 75 μm thick foils interspersed with anode wire banks. Results are compared to simulated outcomes obtained using MCNP6 simulation software for this same geometry under various backfill gas pressures.

2. Theoretical considerations

To predict detector response, MCNP6 was used with detector geometries approximated as 5 parallel sheets of 75 μm thick ^{6}Li foils spaced 1.63 cm apart. P-10 proportional gas (90% Ar, 10% CH_4) was modeled as surrounding the ^{6}Li sheets and was contained within a 1/8 in. thick Al housing. The P-10 pressure was varied to match experimental conditions. A 1.5 cm diameter thermal neutron beam was modeled as normally incident through the center of the MWPC. When a neutron was absorbed, the randomized paths of the reaction products were tracked through the ^{6}Li foil material and the gas. The signal generated by the MWPC was approximated as equal to the energy deposited in the gas by the reaction product(s) as calculated by MCNP6. Electric fields, charge collection, and gas avalanche gain were not modeled.

Because the Li foil thickness (75 μm) is less than the summed range of the triton and alpha particle reaction products (156 μm) several distinct energy depositions characteristic to this type of MWPC can occur, all of which were tracked and calculated. To illustrate the cases, consider Fig. 1, a simple cross-sectional diagram of three Li foils suspended in P-10 gas. There are three situations that allow the reaction products to deposit energy in the gas and produce a measurable event (*i.e.* a pulse). The first such case occurs when both reaction products escape into the gas simultaneously and are measured. A pulse is also produced when only the triton is measured and the alpha particle does not escape the ^{6}Li foil. The probability only the triton is measured is highest among all three events resulting in a measurable electronic pulse and is a result of the long range of the triton (133 μm) compared to the alpha particle range (23.2 μm) in pure ^{6}Li foil [9]. The third characteristic deposition is generated when only the alpha particle is measured, which has the lowest event probability of the three cases for 75 μm thick foils. In the latter two cases, only one reaction product enters in the gas volume, while the other is absorbed in the Li foil. Finally, also illustrated in Fig. 1, both reaction products may be entirely absorbed in the Li foil, thereby, not producing a measurable event. The probability of this last outcome decreases as foil thickness decreases.

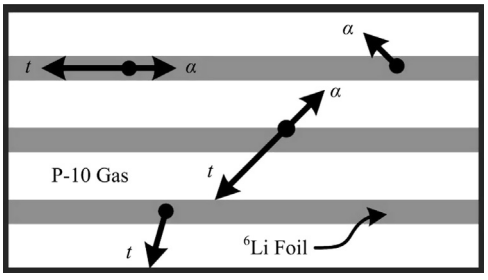

Fig. 1. A cross-sectional diagram of three Li foils suspended in a detector, each separated by P-10 gas. Shown are four basic trajectories for the alpha particle and triton reaction products. Signals are generated from the three basic trajectories that allow reaction products to deposit energy in the P-10 gas.

At 1.0 atm of P-10 gas, the ranges of the 2.73 MeV triton and 2.05 MeV alpha particle are 7.26 cm and 1.25 cm, respectively [9]. In principle the largest pulse will result if all reaction product energy that escapes the foil is deposited in the gas. However, this design for maximum energy deposition would require spacing the lithium foils 7.3 cm apart, a design that is neither practicable nor necessary. As a practical matter, the electronic output pulses need only exceed signal background from electronic white noise and gamma rays. Particles depositing approximately 500 keV of energy or more meet this criterion; hence the detector was designed with foil spacing of 1.63 cm, a distance that allows for the absorption of at least 500 keV from the triton in the gas. Therefore, a 500 keV lower level discriminator (LLD) setting or lower allows for most triton depositions to be counted.

Shown in Fig. 2 are theoretical neutron response pulse-height spectra calculated with MCNP6 for the detector configuration previously described. The pulse-height spectra were calculated for P-10 gas pressures of 1.1, 1.5, 2.0, and 2.8 atm (111, 151, 202, and 284 kPa), revealing the expected spectral changes. The fraction of reaction products measured does not change with gas pressure, but the ranges and energy deposited by each particle and its associated event does vary with pressure. For example, the increase in P-10 gas pressure increases the amount of energy deposited by the triton in the gas region, thereby, resulting in larger pulses. Note that the amount of energy deposited by the alpha particle in the gas volume does not change with increasing P-10 pressure because, at 1.0 atm (101 kPa), the range of alpha particle in the gas is already less than the distance between the ^{6}Li foils. Thus, increasing the pressure only shortens the range of the alpha particle in the gas region and does not increase the energy deposited. Further, the range of the reaction products in P-10 gas changes linearly with pressure. If the pressure is doubled from 1.0 atm to 2.0 atm (101–202 kPa), then the maximum ranges of the reaction products are reduced by approximately 50%.

In the four pulse-height spectra shown in Fig. 2 at the various P-10 gas pressures all have a sharp decrease in count rate at

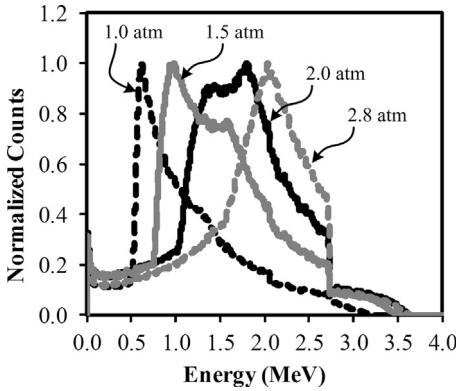

Fig. 2. The simulated thermal neutron pulse-height spectra from a MWPC with five layers of 75 μm thick ^{6}Li foils separated 1.63 cm apart as obtained for P-10 gas pressures of 1.0, 1.5, 2.0, and 2.8 atm (101, 151, 202, and 284 kPa).

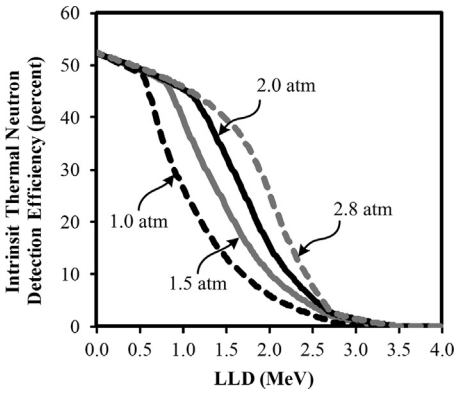

Fig. 3. The intrinsic thermal neutron detection efficiency calculated with MCNP6 for the five layer ^{6}Li foil MWPC as a function of LLD setting for different P-10 gas pressures.

2.73 MeV, which is also the characteristic energy of the triton reaction product. This feature occurs in the spectra when the alpha particle reaction product does not escape the foil and the triton escapes near the surface of the Li foil and deposits all of its energy in the P-10 gas. Similarly, in the 1.0 atm (101 kPa) pulse-height spectra in Fig. 2 there is a small sudden drop in counts at 2.05 MeV, which is the characteristic energy of the alpha particle reaction product. This feature appears in the reverse situation discussed previously; the triton does not escape the Li foil and the alpha particle deposits all of its energy in the P-10 gas volume. Further, because the largest characteristic energy of an individual reaction product is 2.73 MeV, from the triton, counts measured at energies greater than 2.73 MeV can only be generated when both reaction products are depositing energy in adjacent P-10 gas regions simultaneously. However, the pulse-height spectra shapes at all pressures are a result of triton measurement only, which occurs more frequently than the other cases previously described.

The theoretical intrinsic thermal neutron detection efficiency for five layers of 95% enriched ^{6}Li 75 μm thick foils is 55%, and the methodology for determining this efficiency is described elsewhere [6–8]. The efficiency also changes with LLD setting, as shown in Fig. 3, where the intrinsic thermal neutron detection efficiency calculated with MCNP6 is plotted as a function of the LLD setting for each P-10 gas pressure investigated.

The theoretical intrinsic thermal neutron detection efficiency, ε_{th}, is relatively stable for all P-10 pressure settings for LLD settings below 600 keV. At the lowest pressure setting, 1.0 atm (101 kPa), the efficiency decreases with a noticeably greater dependence above 600 keV than observed at higher gas pressures. It is worth noting that the modest efficiency decrease of 4.0% between 0–600 keV is noticeably less than other conventional gas-filled neutron detectors over the same discriminator energy range. The reduced dependence on LLD setting for neutron detection efficiency, as seen for 1.0 atm, is expected from the spectrum shown in Fig. 2. Also, from Fig. 2, for a gas pressure of 1.0 atm, the majority of counts are tallied between 500 keV and 700 keV, beyond which counts decline as eliminated by an increasing LLD. In fact, only 50% of the total initial counts remain when the LLD is set to 1.0 MeV. For higher gas pressures, and the attendant larger electronic pulses, the same effect is observed but at higher LLD settings.

3. Experimental procedure

Li ingots enriched to 95% ^{6}Li were purchased from the Y-12 National Security Complex and rolled into 75 μm thick foils, each 5.0 cm wide, by Rockwood Lithium. The foil strips were positioned five wide onto an Al frame and Cu tape was used at the ends of each foil strip to attach them to the Al frame. A second identical Al frame was placed on top of the foil to sandwich the Li between the two Al frames. This design clamped the perimeter of every Li foil strip. The total frame open area frame was 550 cm^2, approximately 25 cm × 22 cm.

The detectors were assembled by bolting together alternating anode banks and Li foil sheets until a five layer (six anode banks) detector was constructed. The distance between foils was approximately 1.63 cm. The anodes from each bank were linked together and crimped to the lead of an SHV connector. This arrangement gave the option of reading the response of individual banks, or subsets, or all six anode banks together with a single preamplifier. The Li foil and anode stack was fastened to the detector lid. Next, the sub-assembly connected to the lid was lowered into a welded rectangular Al box approximately 30 × 12 × 38 cm^3 composed of 1/8 in. thick aluminum. The lid was bolted to the chamber sandwiching a rubber gasket, thereby, creating a gas-tight seal. The detector was removed from the Ar atmosphere glovebox and purged with P-10 gas; the final pressure was set to 1.1 atm (111 kPa). A slight over-pressure was used to ensure that any pinhole leaks in the detector would not allow oxygen or moisture into the system prior to neutron and gamma-ray sensitivity testing.

The assembled detector, referred to as the 'mid-sized Li foil MWPC', was positioned in the diffracted thermal neutron beam at the KSU TRIGA Mark II nuclear reactor. The reactor power was brought to 10 kW and pulse-height and counting curves were collected to determine an optimal operating voltage for the MWPC. The counting curve exhibited a plateau such that stable operation was observed at 900 V, and this voltage setting was used thereafter.

First, the thermal neutron attenuation (percentage of neutrons absorbed by the detector) was calculated by collecting two 10-min measurements with a calibrated ^{3}He tube (ε_{th}=80.5%) using a normally incident 0.5 cm diameter thermal neutron beam, one measurement with the MWPC detector positioned between the beam port opening and the ^{3}He tube, and the other with the MWPC detector removed. The latter measurement was also used to calculate the intrinsic thermal neutron detection efficiency of the ^{6}Li foil detector. The methodology used to obtain the intrinsic detection efficiency is described elsewhere [6,10]. Pulse-height spectra were also collected for P-10 gas pressures of 1.5, 2.0, and 2.8 atm (151, 202, 284 kPa). Additional efficiency measurements were completed with the detector angled 55° to the neutron beam. During these thermal neutron measurements the detector remained bare without neutron moderator material.

For fast neutron measurements completed with ^{252}Cf, high-density polyethylene (HDPE) was placed around the Li-foil detector. The moderator dimensions were 5.0 cm on the detector front, 10.0 cm on the back, and 2.54 cm thick sheets on the sides, top, and bottom. The absolute neutron detection efficiency in counts per second per ^{252}Cf source mass in nanograms (cps ng^{-1}) of the MWPC was measured with a 10 ng ^{252}Cf neutron source positioned 2.0 m from the front face of the detector. GRRs were calculated using a ^{60}Co gamma-ray source positioned at different distances such that the front face of the detector received exposure rates of 10 and 40 mR hr^{-1}. Additionally, the Gamma Absolute Rejection Ratio in the presence of neutrons (GARRn) was calculated with both neutron and gamma-ray sources present. The characterization methods to determine the absolute detection efficiency, GRR, and GARRn were developed by Pacific Northwest National Laboratories (PNNL) for RPMs, described elsewhere, and were used to obtain the values of the mid-sized Li foil MWPC [11–14].[1]

[1] The required values for a detector to be considered a viable RPM are an absolute efficiency of 2.5 cps ng^{-1} of better, GRR minimum of 1 × 10^{-6}, and GARRn ranging between 0.9 and 1.1.

4. Experimental results

The experimental and simulated pulse-height spectra obtained at P-10 gas pressures of 1.1, 1.5, 2.0, and 2.8 atm are shown in Figs. 4–7, respectively. The energy scale originates from the simulation and allowed for energy calibration of the experimental data.

At 1.1 atm (111 kPa) P-10 gas pressure, the measured thermal neutron attenuation was $75.1 \pm 0.31\%$, and the intrinsic thermal neutron detection efficiency of the Li foil MWPC was measured to be $53.8 \pm 0.20\%$ with the LLD set at 450 keV. The thermal neutron detection efficiencies for the 1.5, 2.0, and 2.8 atm (151, 202, 284 kPa) pressure settings were all within 1.0% of each other and were 53.3%, 53.0%, and 52.9%, respectively, and had less than 1.0% error. When the detector was oriented at 55° to the neutron beam, the intrinsic thermal neutron detection efficiency increased to $58.6 \pm 0.21\%$.

The detector was also tested at Saint-Gobain Crystals (SGC) using calibrated ^{252}Cf and ^{60}Co sources. Shown in Fig. 8 is a pulse-height spectrum acquired when the detector was exposed to a 10 ng ^{252}Cf source positioned 2.0 m from the front moderator of

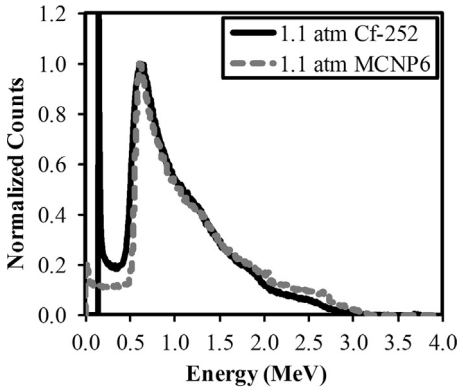

Fig. 4. The simulated (gray dashed) and measured (solid black) thermal neutron response spectra for the five-layer ^{6}Li-foil MWPC obtained at a P-10 gas pressure of 1.1 atm.

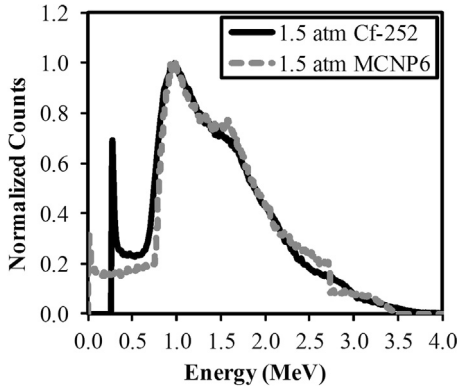

Fig. 5. The simulated (gray dashed) and measured (solid black) thermal neutron response spectra for the five-layer ^{6}Li-foil MWPC obtained at a P-10 gas pressure of 1.5 atm.

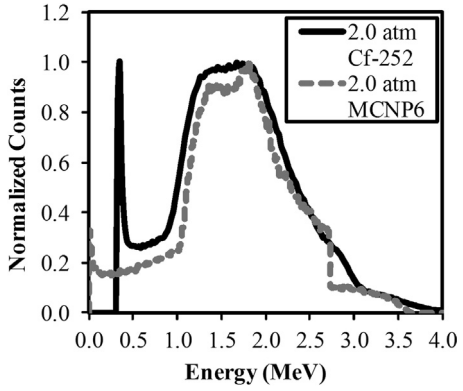

Fig. 6. The simulated (gray dashed) and measured (solid black) thermal neutron response spectra for the five-layer ^{6}Li-foil MWPC obtained at a P-10 gas pressure of 2.0 atm.

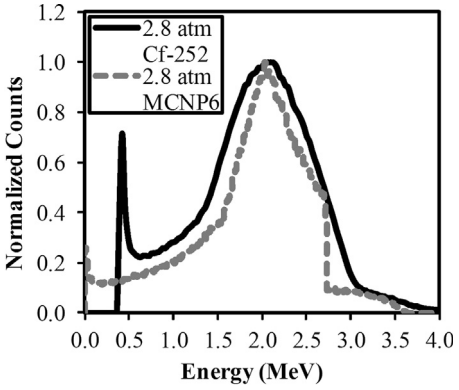

Fig. 7. The simulated (gray dashed) and measured (solid black) thermal neutron response spectra for the five-layer ^{6}Li-foil MWPC obtained at a P-10 gas pressure of 2.8 atm.

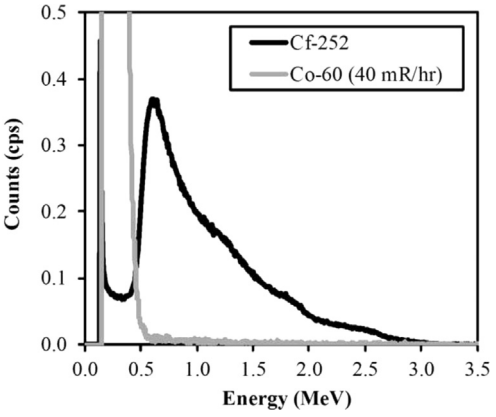

Fig. 8. The measured pulse-height spectra collected separately from the ^{252}Cf neutron source (black) and a ^{60}Co gamma-ray source (gray) at an exposure rate of 40 mR hr^{-1}.

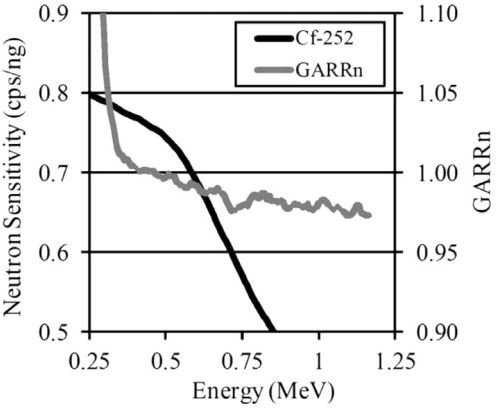

Fig. 9. The absolute neutron detection efficiency (black) and GARRn measurement (gray) plotted as a function of LLD setting. The GARRn measurement was made in a 10 mR hr^{-1} ^{60}Co field.

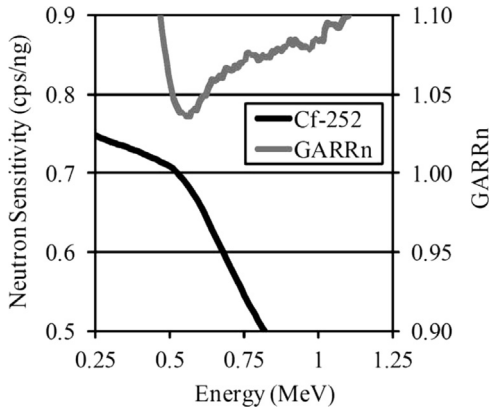

Fig. 10. The absolute neutron detection efficiency (black) and GARRn measurement (gray) plotted as a function of LLD setting. The GARRn measurement was made in a 40 mR hr^{-1} ^{60}Co field. The increase of the GARRn out of the acceptable range is a consequence of the short counting time used for the background measurement.

the detector. Also shown in Fig. 8 is a spectrum obtained with a ^{60}Co (40 mR hr^{-1}) source present. Spectra were also recorded with both sources present. The absolute neutron detection efficiency measured at SGC was 0.73 cps ng^{-1} with an LLD setting of 500 keV. The GRR calculated with a 40 mR hr^{-1} exposure rate was 7.67×10^{-9} with the same LLD setting, exceeding RPM requirement. The associated GARRn calculated with 10 mR hr^{-1} and 40 mR hr^{-1} exposure rates were 0.997 and 1.07, respectively, within the accepted range. Shown in Figs. 9 and 10 is the neutron sensitivity and GARRn as a function of LLD setting for the 10 mR hr^{-1} and 40 mR hr^{-1} exposures, respectively.

5. Discussion

Examination of Figs. 4–7 indicate that the MCNP6 predicted pulse-height spectra match well to the experimental results. The accuracy of the simulations yields confidence that such simulations are useful predictors for responses of additional detector geometries. The sharp structures in the simulated results are from the supposition that all energy deposited in the gas contributes to the pulse height with equal contribution, in other words, no charge collection differences from electric field variations or detector geometry were included in the simulation. These other influences smear the experimental results from the simulated results. Also, electronic noise adds to uncertainty and spectral 'smearing' in the experimental data. For example, the sudden drop in counts at 2.73 MeV in the simulated pulse-height spectra does not appear as defined in the experimental data due to the resolution of the detector. Even so, the salient features from the simulation are present in the measured results.

At 1.1 atm (111 kPa), the experimental results are nearly a perfect match to the simulation. The overlap between the simulated and measured pulse-height spectra is greatest for the 1.1 atm (111 kPa) P-10 gas pressure compared to the higher gas pressures investigated. Additionally, the spectral features appearing in the predicted pulse-height spectra are more easily identifiable at lower P-10 gas pressures. In general, the discrepancies between the simulated and measured pulse-height spectra increase as P-10 gas pressure is increased. Raising the gas pressure reduces charge carrier mobility, which consequently reduces charge carrier velocity. Because all measurements were conducted at 900 V, the velocity, and consequent charge collection, reduced as gas pressure increased.

The pulse-height spectra of the 1.1, 1.5, 2.0, and 2.8 atm (111, 151, 202, 284 kPa) P-10 pressures all have pronounced valleys between the main feature and the electronic noise. The gamma-ray response decreases to a minimal response in this 'valley' region as shown in Fig. 8, which is excellent for gamma-ray discrimination, as shown by the GRR and GARRn. Within the 'valley' region, the LLD can be adjusted to an energy setting that exceeds the gamma-ray response with negligible loss in neutron detection efficiency. The intrinsic thermal neutron detection efficiency decreased less than 2% when the LLD was raised from 300 keV to 500 keV, an expected result predicted by the simulations.

The MWPC with the layered ^{6}Li foil construction is a promising geometry for portal monitoring detectors, as shown by the absolute neutron detection efficiency and excellent gamma-ray rejection. To meet typical absolute efficiency requirements, the detector area must be increased from 550 cm^2 to approximately 2200 cm^2. The increase in area can be accomplished by constructing larger units or by connecting multiple units. The GRR exceeded the minimum requirement of 1×10^{-6} by more than two orders of magnitude, and the GARRn falls almost exactly in the middle of the acceptable range (0.90–1.10). These gamma-ray results are not expected to change significantly with an increase in area, although pulse pile-up may become a factor as detector height increases. Additionally, the thickness of the detector must be decreased in order for the device to fit current RPM dimensions [13].

However, the detector described here was delivered to a government sponsored backpack neutron detector test campaign where the performance of the device was compared to current available ^{3}He backpack neutron detectors. Approximately 0.25 in. of HDPE was positioned on the sides, top, and bottom of the detector, while 0.75 in. was placed on the back of the Li foil MWPC. Further, custom transistor-transistor logic (TTL) output electronics were included, and the electronics and detector together weighed 24 lbs. Results from the tests revealed the Li foil MWPC backpack neutron detector performed better than currently available ^{3}He backpack detectors. Thus, the Li foil MWPC backpack neutron detector was accepted as a viable ^{3}He replacement.

The observed increase in intrinsic thermal neutron detection efficiency when the detector was angled at a 55° resulted from increased neutron absorption. At 55° from normal, the path length increases to approximately 125 μm of ^{6}Li foil, rather than 75 μm when normally incident, and the theoretical thermal neutron attenuation through the ^{6}Li foils increases from 76.5% to 88.7%. The reaction product escape probabilities remain unchanged, and the theoretical efficiency shows an increase from 55% to 66% for this angle change. However, the measured efficiency at 55° had a lower difference by 13%. This difference is believed to be a consequence of masking and scattering effects from the detectors internal structure. Intrinsic thermal neutron detection efficiency reaches maximum at approximately 75°, and would theoretically be 70.9%.

6. Conclusions

The ^{3}He gas shortage for neutron detection has raised interest in alternative neutron detection technology. A mid-sized ^{6}Li foil MWPC neutron detector with five layers of ^{6}Li foil covering an area of 550 cm^2 yielded an intrinsic thermal-neutron detection efficiency of 53.8%, an absolute efficiency of 0.73 cps ng^{-1} for ^{252}Cf at 2.0 m, and gamma-ray discrimination typical of gas counters (equivalent or better than some ^{3}He tubes). These measured properties suggest that the technology is a viable ^{3}He replacement detector. It is expected that the absolute efficiency can be increased by arraying detectors together, or by making them larger. Further, the intrinsic thermal neutron detection efficiency can be increased by adding additional ^{6}Li foil layers.

Acknowledgments

This work was supported in part by the U.S. Defense Threat Reduction Agency (DTRA), under contract HDTRA1-12-c-0002. The authors express their gratitude to the KSU TRIGA Mark II nuclear reactor staff for their helpful assistance.

References

[1] S.L. Bellinger, D.S. McGregor, W.J. McNeil, K.A. Nelson, M.F. Ohmes, Gas-filled neutron detectors having improved detection efficiency, US. Pat. 8519350, August 26, 2013.
[2] S.L. Bellinger, D.S. McGregor, K.A. Nelson, Gas-filled Neutron Detectors and Imaging System and Array of Such Detectors, PCT. Appln. No. PCT/US2013/0228696, February 22, 2013.
[3] N. Tsoulfanidis, Measurement and Detection of Radiation, 2nd Edition, Taylor and Francis, New York, 1995.
[4] G.F. Knoll, Radiation Detection and Measurement, 3rd Edition, Wiley, New York, 2000.
[5] N. D'Olympia, P. Chowdury, C.J. Lister, J. Glodo, R. Hawrami, K. Shah, U. Shirwadkar, Nuclear Instruments and Methods A 714 (2013) 121.
[6] K.A. Nelson, S.L. Belling, B.W. Montag, J.L. Neihart, T.A. Riedel, A.J. Schmidt, D.S. McGregor, Nuclear Instruments and Methods A 669 (2012) 79.
[7] K.A. Nelson, S.L. Bellinger, B.W. Montag, J.L. Neihart, T.A. Riedel, A.J. Schmidt, D.S. McGregor, IEEE Transactions on Nuclear Science N20-2 (2011) 1026.
[8] D.S. McGregor, M.D. Hammig, Y.-H. Yang, H.K. Gersch, R.T. Klann, Nuclear Instruments and Methods A 500 (2003) 272.
[9] J. Ziegler, J. Biersack, Stopping Ranges of Ions in Matter (SRIM), Version, 2008.
[10] D.S. McGregor, J.K. Shultis, Nuclear Instruments and Methods A 632 (2011) 167.
[11] R.T. Kouzes, PNNL-18388, 2009.
[12] R.T. Kouzes, J.H. Ely, PNNL-19360, 2010.
[13] R.T. Kouzes, J.H. Ely, L.E. Erikson, W.J. Kernan, A.T. Lintereur, E.R. Siciliano, D.L. Stephens, D.C. Stromswold, R.M. Van Ginhoven, M.L. Woodring, Nuclear Instruments and Methods A 623 (2010) (2010).
[14] R.T. Kouzes, J.H. Ely, L.E. Erickson, W.J. Kernan, A.T. Lintereur, E.R. Siciliano, D.C. Stromswold, M.L. Woodring, PNNL-19311, 2010.